Open Peer Review on Qeios

RESEARCH ARTICLE

A Computer Simulation Study on Ion Optics Aiming at the Realization of Projection-Type Mass Spectrometry Imaging

Yasuhide Naito[1]

1 Graduate School for the Creation of New Photonics Industries, Hamamatsu, Japan

Funding: No specific funding was received for this work.

Potential competing interests: No potential competing interests to declare.

Abstract

The projection mode in mass spectrometry imaging (MSI) obtains ion images by retaining the spatial distribution of desorbed ions immediately after their generation as the ion images, then projecting them onto an ion detector of time-of-flight mass spectrometry. Compared to conventional MSI, projection-type MSI can deliver overwhelmingly higher spatial resolution. The mass resolution of projection-type MSI can be improved by a technique named post extraction differential acceleration (PEDA). To assess the feasibility of projection-type MSI with minimal modification of a commercially available laser desorption/ionization time-of-flight mass spectrometer, ion trajectory simulations were performed using the ion optics simulation program SIMION. Under boundary conditions that reproduce the ion acceleration region of the commercial mass spectrometer with a high fidelity, the trajectory simulation results were obtained for a huge number of combinations of ion masses, initial conditions, PEDA parameters, etc. The data analysis provided useful findings that can lead to the realization of projection-type MSI based on the modified commercial mass spectrometer, for instance, the imaging conditions for ion images in the commercial equipment, guidelines for optimizing PEDA parameters, and the effects of differences in PEDA high-voltage rising waveforms.

1. Introduction

Mass spectrometry imaging (MSI) is an analytical technology for obtaining a chemical mapping of a sample surface by specifying chemical species present on the sample surface using mass spectrometry along with visualizing their spatial distributions as images[1]. Applications of MSI are spreading not only in researches of such as life sciences and materials science, but also in a wide range of industries including pharmaceutical and semiconductor industries. A general method of MSI utilizes local desorption of chemical species from a micro area of the sample surface induced by a focused-beam, often ionization of the species occurs in parallel. By repeating mass analysis of the ionic species accompanied with the positional information of desorption over an observation area on the sample surface, chemical mapping of the observation area can be obtained.

Matrix-assisted laser desorption/ionization (MALDI), which uses laser light as the desorption-inducing beam, is a soft

ionization method, and MALDI-MSI can perform chemical mapping of molecular species, including labile macromolecules such as proteins[2]. The spatial resolution of early MALDI-MSI was several hundred microns. However, thanks to technological improvements such as increasing the repetition rate of the laser light sources and generating beam profiles that do not impair ionization efficiency even when the focused spot is reduced, it is now possible to routinely achieve a spatial resolution of approximately 10 μm[3].

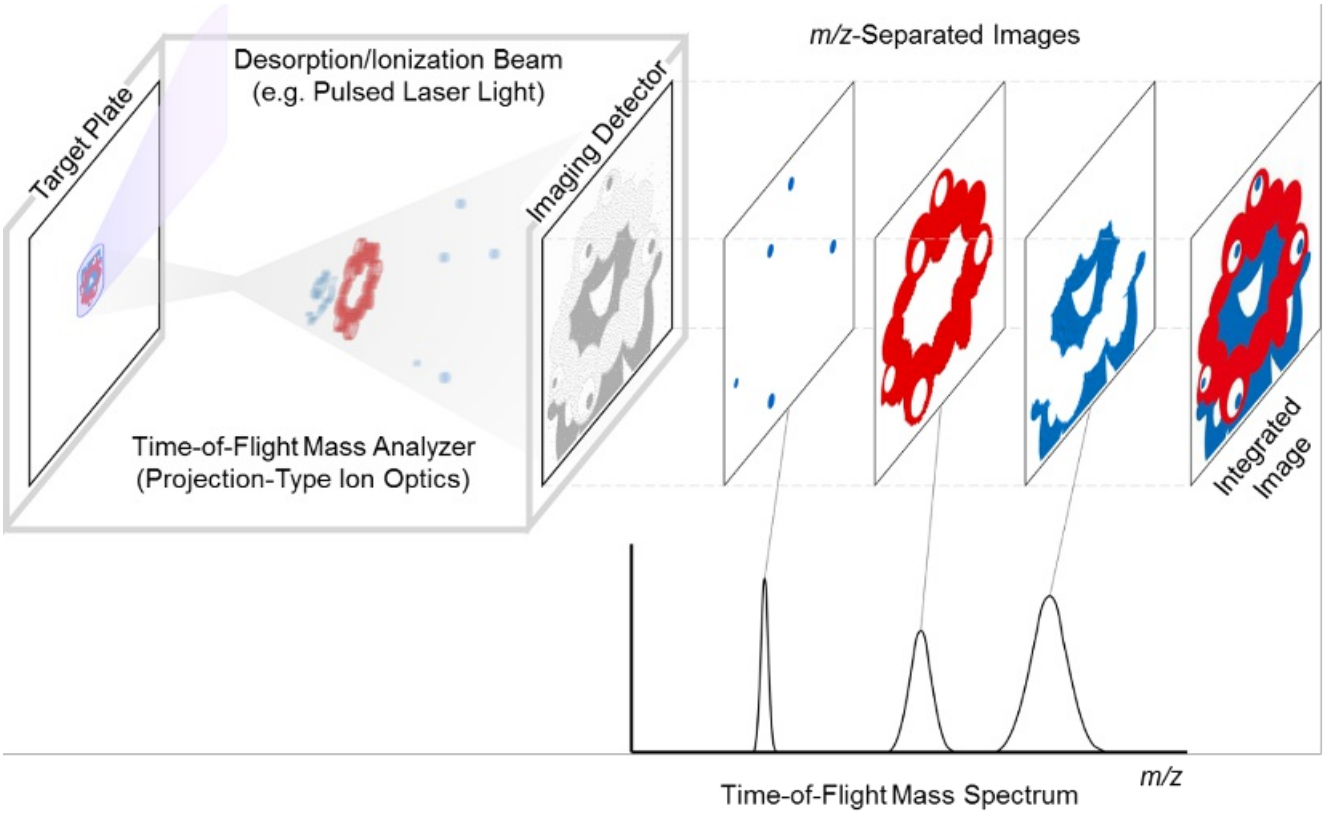

Figure 1. Schema of projection-type mass spectrometry imaging. Extract electrode is omitted in the drawing. (MYAKU-MYAKU; Expo 2025 Osaka Kansai official character)

Projection-type MSI[4][5][6] also known as the microscope type or stigmatic type, treats the desorbed and ionized chemical species as ion images while retaining their spatial distributions within the irradiation spot of the desorption beam, and acquires the ion images by projecting them through an electrostatic lens onto a position-sensitive ion detector[7][8] or imaging ion detector[9][10][11] placed on the imaging plane (Fig. 1). The behavior of the ion trajectories at this time exhibits analogy to the behavior of light rays in a camera optics system constructed with optical lenses. Besides, the ion source including an electrostatic lens as a component is basically equivalent to an ion acceleration region in a time-of-flight mass spectrometer. It is therefore possible to project mass-separated ion images based on their flight times. In other words, projection-type MSI can be realized only with time-of-flight mass spectrometry (TOFMS). While the spatial resolution of conventional MSI is limited by the irradiation spot size of the desorption beam, the spatial resolution of projection-type MSI does not have such limitation. That means, a local area that is treated as a "point" on the sample surface in conventional MSI is treated as an "area" in projection-type MSI. Even though the spatial resolution of MALDI-MSI has improved significantly through incremental improvements, the significance of the projection mode in MSI remains distinct

— it will bring about disruptive innovation in the spatial resolution of MSI.

Although the concept of projection-type MSI was proposed a long time ago[12] there have only been research examples by a few groups, and no commercially available equipment has emerged or become widespread to date. Relying solely on TOFMS would be a major disadvantage in terms of analytical specificity. Furthermore, in general TOFMS, mass resolution is usually improved by a delay between generation and extraction/acceleration of ions, but projection-type MSI is inadaptable to this since it becomes impossible to retain ion images.

A group from Osaka University has proposed a method called post extraction differential acceleration (PEDA) that delivers the same effect in projection-type MSI as delayed extraction, thereby improving the mass resolution (Fig. 2).[13] In PEDA, a steady acceleration voltage is applied on the first acceleration region between the target plate and the extract electrode. As a result, the spatial distributions of ions immediately after their generation are retained as ion images, and the first acceleration region works properly as an electrostatic lens. At the time when the flight distances of the ions have sufficiently dispersed in the second acceleration region between the extract electrode and the ground electrode due to their initial velocity dispersion, the potential applied to the extract electrode is instantly pulled up. That is, delayed extraction uses the first acceleration region for compensating the initial velocity dispersion, whereas PEDA uses the second acceleration region for it. Adjustment of the instrumental parameters V_{PEDA} and t_{delay} is the condition for PEDA to work properly. Unlike delayed extraction, PEDA compensates the initial velocity dispersion of ions that have already been accelerated and begun to be mass-separated, so the mass range over which a certain operating condition is effective is much narrower than in the case of delayed extraction. A group from the University of Oxford has proposed two-stage PEDA to extend the effective mass range.[14]

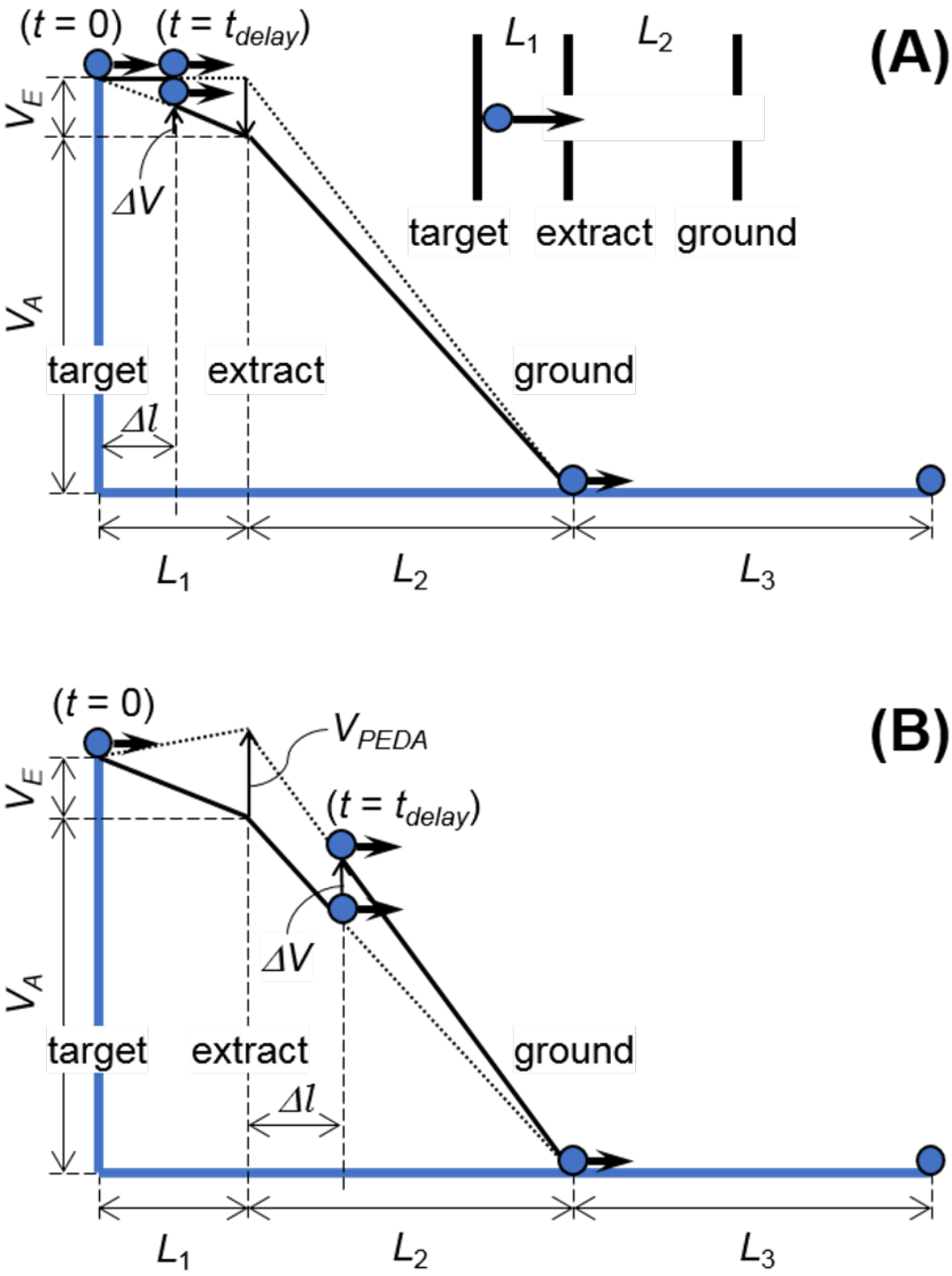

Figure 2. Potential surfaces of (A) a conventional delayed extraction; DE, and (B) a single-stage post extraction differential acceleration; PEDA. Solid and dotted lines indicate before and after voltage switching, respectively. In both the cases, the relationship between the flight distance Δl and acceleration voltage increment ΔV (longer Δl lower ΔV) is responsible to the correction of initial velocity dispersion.

This study aims to realize a projection-type MSI based on a commercially available laser desorption/ionization time-of-flight mass spectrometer, Ultraflex (Bruker, Germany). It is intended that modifications will be kept to a minimum, except for replacing the ion detector that detects ion signals providing only time-of-flight information with an ion detector that also provides positional information. PEDA will be implemented by diverting the pulsed high-voltage power supply for pulsed

ion extraction (equivalent to delayed extraction) of Ultraflex. To assess the feasibility of projection-type MSI based on this minimally modified commercial equipment, ion trajectory simulations were carried out by using an ion optics simulation program SIMION 3D ver. 7.0 (Bechtel Bwxt Idaho, LLC, USA). The issues to be clarified through this simulation study are the following four:

> Is it possible to achieve ion image formation and magnification on the ion detector surface with reasonable electrode potential settings without changing the ion source electrode configuration of the Ultraflex?

> Can PEDA be fully effective using the actual high-voltage rising waveform with a finite time constant delivered from the pulsed high-voltage power supply?

> Is it possible to obtain useful guidelines for adjusting the mass-dependent PEDA parameters (V_{PEDA}, t_{delay})?

> Do the conditions under which PEDA is fully effective not affect the proper formation of ion images?

2. Computational Methods

2.1. Creation of Potential Arrays

To simulate the linear-mode time-of-flight mass spectrometer, two potential array instances, representing the ion source and the ion detector, were created.

The potential array of the ion source is based on the actual structure and dimensions obtained by removing the electrode assembly from the interior of the Ultraflex ion source and measuring it (Fig. 3). The size of the domain in which the array geometry was defined is 1000 by 100 grid units, and the potential array was defined as a 2D array with cylindrical symmetry about the *x*-axis. The electrodes are arranged along the *x*-axis, and the left end ($x = 0$ side) is the target plate. The potential array instance, which is the volume of revolution about the *x*-axis generated from the 2D array, reproduces with sufficient fidelity the region near the central axis that contributes to the formation of ion trajectories in the Ultraflex ion source (Fig. 4). In the actual Ultraflex ion source, the cylindrical electrode following the ground electrode is applied with a variable potential so that it can function as an Einzel lens. However, in this simulation, the Einzel lens potential was fixed at 0 V to simplify the conditions for the study. Therefore, only the target plate and the extract electrode were made variable potential electrodes, i.e., electrodes that could utilize the Fast Adjust features of SIMION.

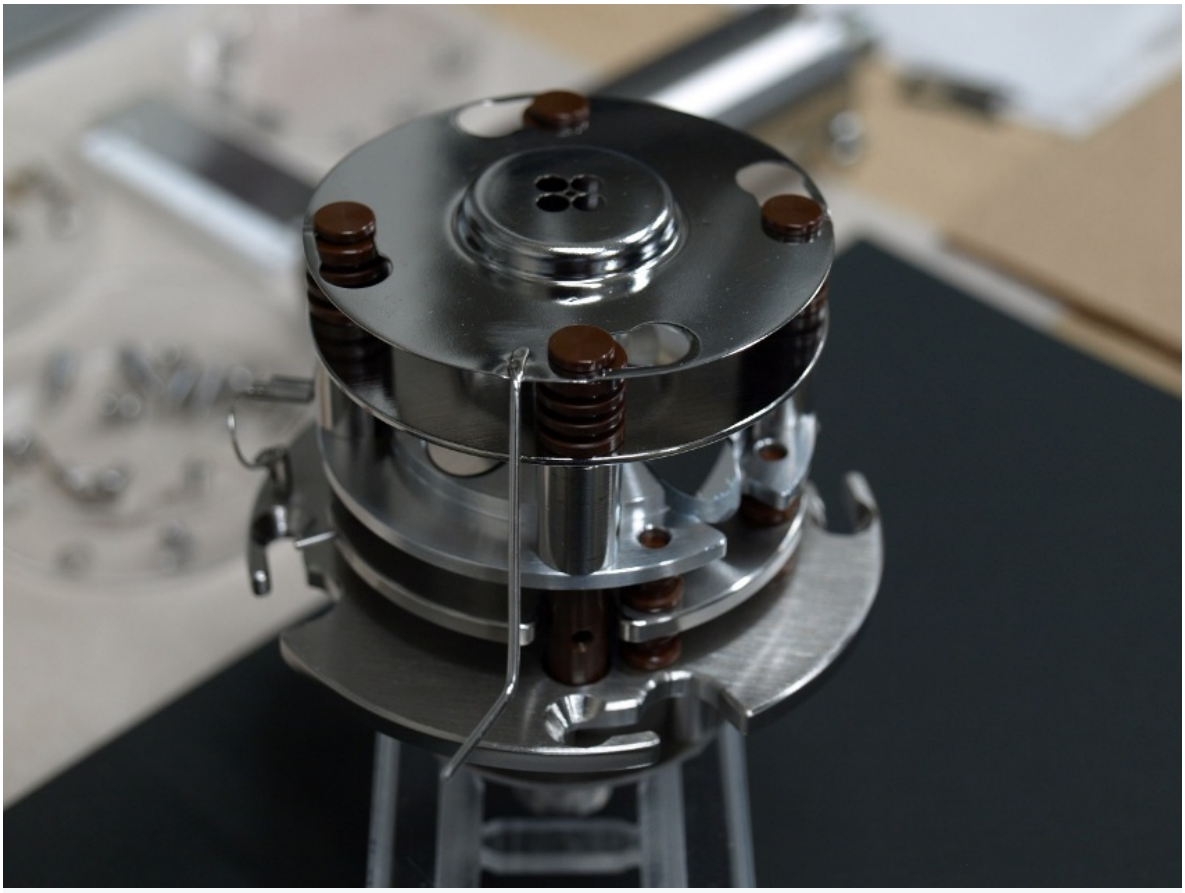

Figure 3. The electrode assembly of ion accelerating region removed from Ultraflex ion source interior.

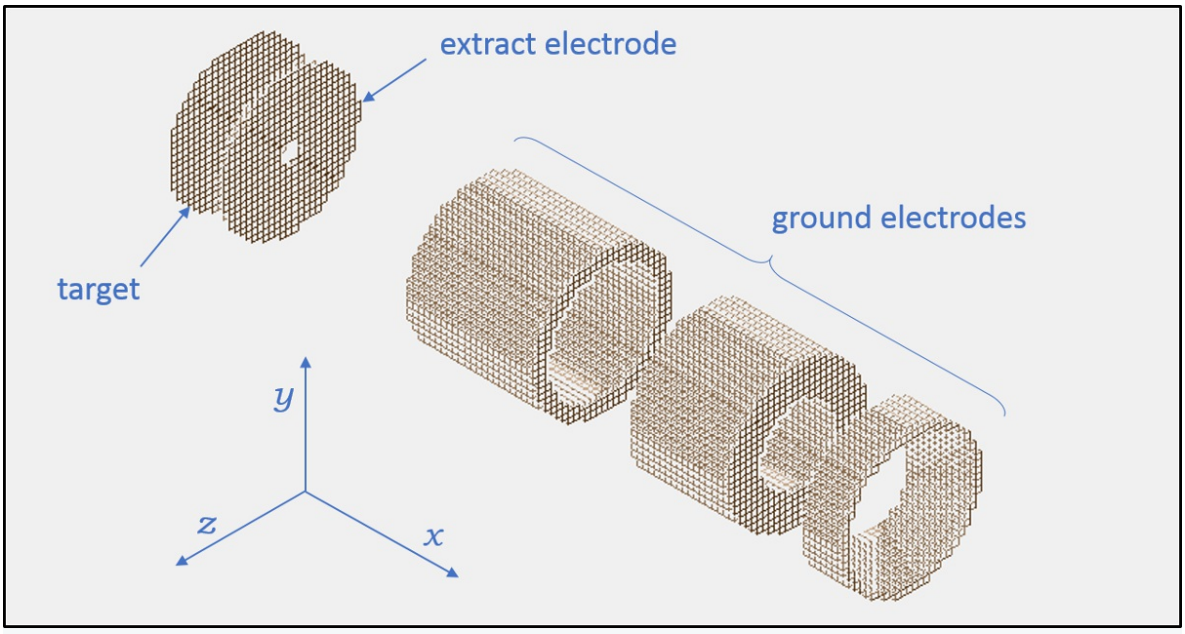

Figure 4. The potential array instance corresponding to the ion source electrodes.

The potential array of the ion detector is a flat disk with a diameter of 30 mm based on the circular microchannel plate entrance surface of the expected imaging ion detector. The 2D array was defined in a domain of 10 by 149 grid units with cylindrical symmetry about the *x*-axis. The potential was fixed at 0 V. Using SIMION's user programming features, it was

implemented a function that the final position coordinates (*y* and *z* on the SIMION ion optics workbench) and the arrival time (= flight time) are stored in separate ASCII format files every time an ion trajectory simulation is run.

The SIMION ion optics workbench volume was sized to correspond to the actual scale of the Ultraflex time-of-flight mass spectrometer. The potential array instances were placed on the ion optics workbench so that the orientation of the coordinate axes of each instance matched the coordinate system of the ion optics workbench. The scaling factors were set for the potential array of the ion source, 1 grid unit = 0.05 mm, and for the potential array of the ion detector, 1 grid unit = 0.1 mm. The distance from the target plate surface to the ion detector surface was set to 2290 mm based on the measurement of the actual dimension.

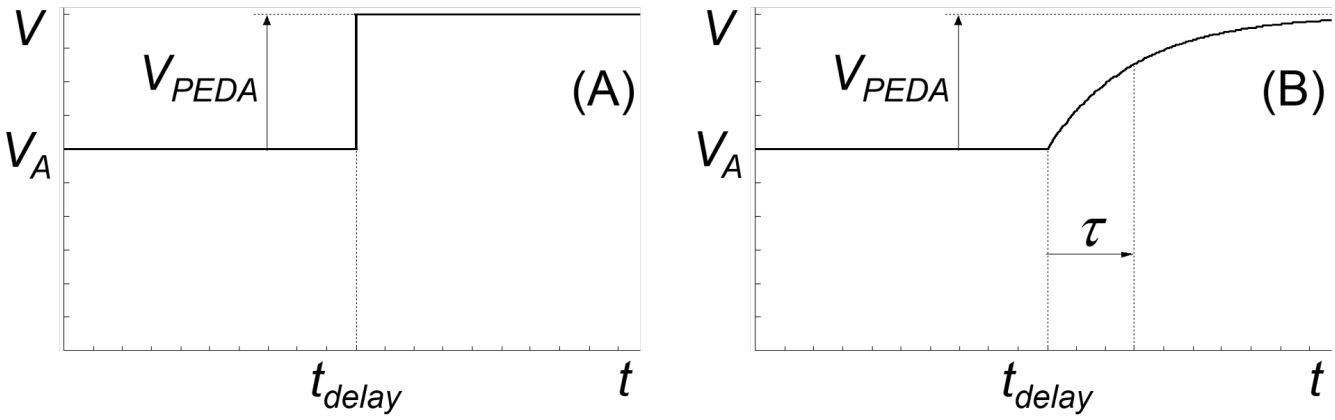

Figure 5. The extract potential rising waveforms used for the present simulation study. (A) The "ideal" step function waveform. (B) The "realistic" exponentially rising waveform. The latter is expressed by:

$$V = V_A \qquad \left(t < t_{\text{delay}}\right)$$

$$V = V_A + V_{\text{PEDA}}\left(1 - \exp\left(\frac{t_{\text{delay}} - t}{\tau}\right)\right) \qquad \left(t \geq t_{\text{delay}}\right)$$

2.2. Implementing PEDA into Simulation

The operation of PEDA, which switches the extract electrode potential at a predetermined timing during an execution of an ion trajectory simulation, was implemented using SIMION's user programming features. In the initial state, the extract electrode is applied with a potential V_2 slightly lower than the target plate potential V_1. After ions have passed through the extract electrode, the extract electrode potential is gradually pulled up toward $V_2' = V_2 + V_{\text{PEDA}}$ at a delay time t_{delay}, a timing from the ion generation, as the onset (Fig. 5). This transient change was modeled as an exponentially rising waveform with a time constant of $\tau = 30$ ns. The value of the time constant was determined based on observation of the actual output voltage waveform delivered from the Ultraflex pulsed high-voltage power supply, which will be diverted for the PEDA power supply.

For comparison with the above "realistic" simulations in which the extract electrode potential rises exponentially, the PEDA operation in the case where the change in the extract electrode potential is modeled as an "ideal" step function was also

implemented by user programming. In this case, a program process was performed to adjust the simulation time step immediately before t_{delay} so that the ion trajectory integration step was executed in exact agreement with the timing at which the extract electrode potential was instantly switched.

2.3. Group Definitions of Ions and Initial Conditions

In TOFMS, flight times of ions are proportional to the square root of *m/z* values. Therefore, the masses of the ions to be simulated were set to 100 Da, 400 Da, 900 Da, and 1600 Da so as to be equally spaced on the axis of flight time, and all were defined as singly charged positive ions. In addition, to investigate the influence due to small differences in mass within each mass region, six different masses were added in the range of ±30 Da to ±120 Da for each mass region. Resultantly a total of 28 different singly charged positive ions were subjected for the trajectory simulations.

Table 1. Initial conditions of simulated ion trajectories

Location (y_0, z_0) **[µm]**	**Direction** (*El*, *Az*) **[degree]**	**Velocity**† v_0 **[m s^{-1}]**
(0, 0)	(0, 0) (0, 40)	439.3314, 621.3084, 760,9442, 878.6627, 982.3748, 1076.138,
(0, 100)	(0, 0) (0, 40) (0, –40)	1162.362, 1242.617, 1317.994, 1389.288, 1457.097, 1521.888,
(0, 200)	(0, 0) (0, 40) (0, –40)	1584.032, 1643.827, 1701.523, 1757.325, 1811.410, 1863.925, 1915.001, 1964.750

†*Defined as kinetic energy for each mass*

Initial conditions for the ion velocities were defined considering a broad distribution with a mean value of about 10^3 m s^{-1} that is almost independent of the ion mass[15]. The magnitudes of the initial ion velocities were set to 20 levels in the range of 439–1965 m s^{-1} equally for all masses. For each mass, ions with this initial velocity range were defined as a group of ions. In SIMION, initial conditions of ion motion are set by kinetic energy rather than velocity. Therefore, the start value and increment of the initial kinetic energies within a definition group of ions were adjusted according to mass to fulfill the same initial velocity range for all groups. For example, the start value and increment were 0.07 eV for 70 Da, and for

1720 Da they were 1.72 eV.

The initial locations (y_0, z_0) and starting directions (*El*, *Az*) of ions were defined as the eight combinations shown in Table 1. Taking into account the cylindrically symmetric boundary condition, only z_0 and the elevation angle *Az* relative to the *z*-axis were defined as parameters. That is, eight definition groups of ions were set for each mass.

Table 2. PEDA settings

Mass [Da]	t_{delay} [ns]	V_{PEDA} [V]	Rising waveform
70–130 (at 10 Da intervals)	140, 150, 160, 170, 180, 190, 200, 210, 220, 230, 240, 250	200, 250, 300, 350, 400, 450, 500, 550, 600	Exponential function Step function
340–460 (at 20 Da intervals)	360, 370, 380, 390, 400, 410, 420, 430, 440, 450, 460, 470		
810–990 (at 30 Da intervals)	590, 600, 610, 620, 630, 640, 650, 660, 670, 680, 690, 700		
1480–1720 (at 40 Da intervals)	820, 830, 840, 850, 860, 870, 880, 890, 900, 910, 920, 930		

About the PEDA parameters, V_{PEDA} was set to nine levels in the range of 200–600 V, and t_{delay} was set to 12 levels with the range adjusted to each mass region (Table 2). About the PEDA high-voltage rising waveforms, the exponential and step functions were examined. In addition, the case where PEDA was turned off was also included as a reference condition for all ions. Therefore, in total, ion trajectory simulations were performed for 28 20 8 (9 12 2 + 1) = 972160 different conditions.

2.4. Simulation Running and Post-Processing

Because this study requires an enormous number of simulation runs, only the z-displacements at the end of trajectories and flight times were analyzed as the final states, instead of the entire trajectories. The trajectory quality (later mentioned) was set to 3. The contents of the ASCII format files of the final states created for each simulation run were copied into spreadsheets for tabulation and analysis of data. MATLAB ver. 5.3 (MathWorks, USA) was used to graphically display the analysis results.

3. Results and Discussion

3.1. Determining the Imaging Condition

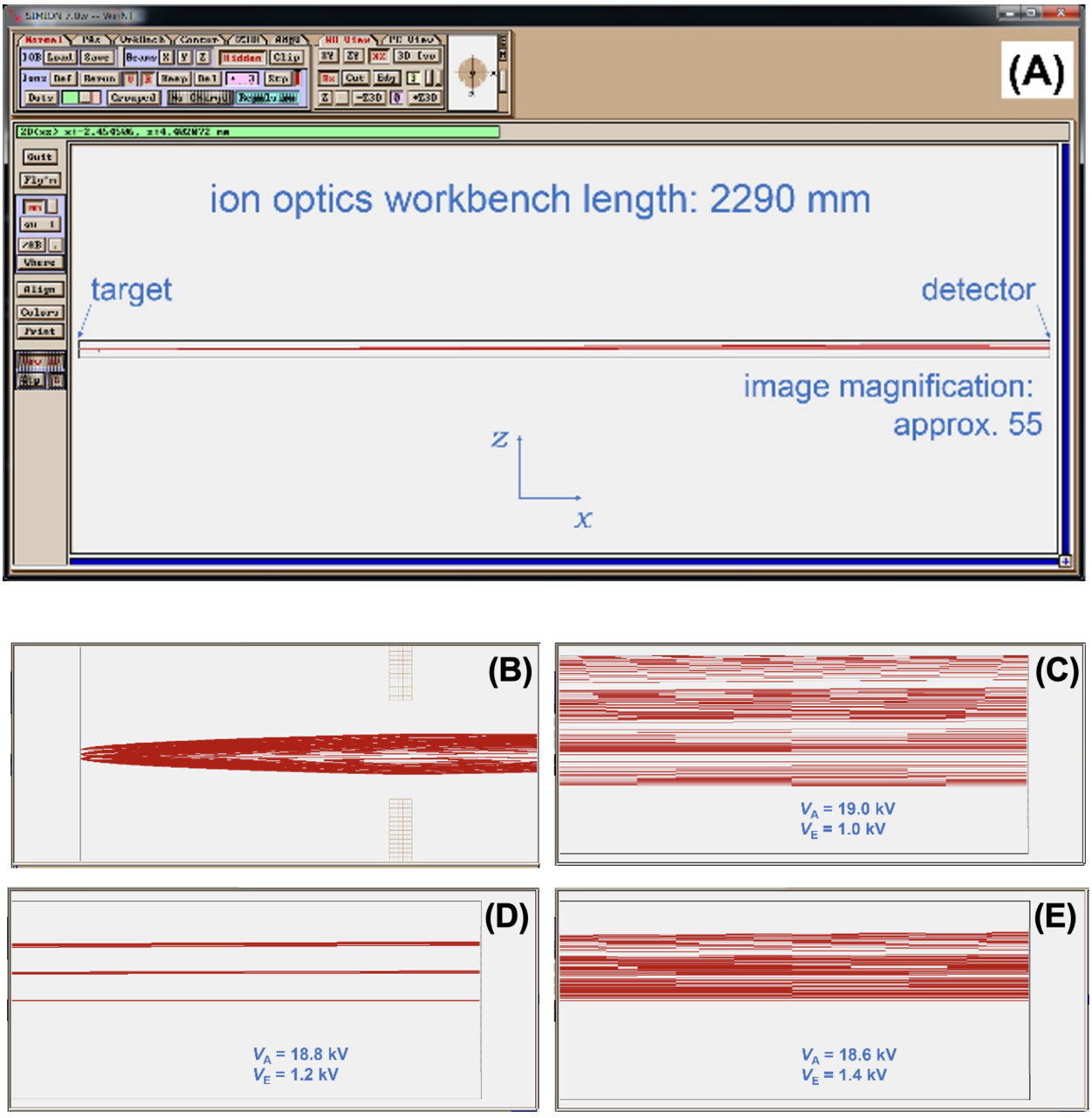

Figure 6. Ion trajectories (red lines) calculated for determining the imaging condition of the projection-type MSI ion optics in

simulation. (A) Trajectories displayed in the entire ion optics workbench. (B) Enlarged view of around the target. (C–E) Enlarged views of around the detector, for various settings of the electrostatic lens potentials without PEDA.

First, the ion extraction voltage V_E, which has the greatest effect on the ion image formation, was optimized by simulating the ion trajectories without PEDA. The target plate potential (ion acceleration voltage) V_1 was fixed at 20 kV, a typical experimental value, and the extract electrode potential V_2 was varied as a parameter. The ion extraction voltage is given by $V_E = V_1 - V_2$.

An example of the simulation results is shown in Figure 6. Figure 6A shows the entire ion optics workbench, Figure 6B shows an enlarged view of the vicinity of the potential array instance corresponding to the target plate and the extract electrode, and Figures 6C–6E show enlarged views of the vicinity of the potential array instance corresponding to the ion detector. The calculated ion trajectories are displayed as red lines. The trajectories of ions emitted from a starting point on the target plate immediately spread due to a dispersion of the initial velocity orientation (Fig. 6B). If they converge to a point on the detector, they are in the image-formed state. In Figures 6C (V_E = 1 kV) and 6E (V_E = 1.4 kV), the ion trajectories are spreading on the detector, whereas in Figure 6D (V_E = 1.2 kV) the ion trajectories are almost converging to a point on the detector. However, even in this case, complete point convergence is not achieved. In particular, ion trajectories with large initial displacements z_0 are less focused. It is considered that the electrostatic lens formed by the target plate and the extract electrode has the ion optical aberration of a substantial magnitude. However, since this convergence state was the best, V_E = 1.2 kV, i.e., V_2 = 18.8 kV, was determined as the imaging condition. The image magnification was approximately 55 for singly charged ions of 100 Da.

When PEDA is turned on, the extract electrode potential switches to $V_2' = V_2 + V_{PEDA}$ after t_{delay} from the time of ion generation. Even in this case, the extract electrode potential is maintained at V_2 = 18.8 kV during the period ($t < t_{delay}$) when the ions fly between the target plate and the extract electrode, so the imaging condition is considered to be maintained.

3.2. Time-of-Flight Focusing with PEDA

Next, the effect of PEDA on improving the time-of-flight dispersion ΔTOF caused by the initial velocity distribution was assessed by simulating the ion trajectories with PEDA turned on. Figure 7 shows 3D plots of the simulation results for singly charged ions ranging from 70 Da to 130 Da. The horizontal axes represent the two parameters V_{PEDA} and t_{delay}, and the vertical axis represents the ratio $R_{\Delta TOF}$.

$R_{\Delta TOF}$ = (ΔTOF without PEDA) / (ΔTOF with PEDA)

Where, the regions in red of the color scale corresponding to the highest $R_{\Delta TOF}$ value indicate the highest effect of PEDA on time-of-flight focusing. It can be seen that the red region varies even in this narrow mass range.

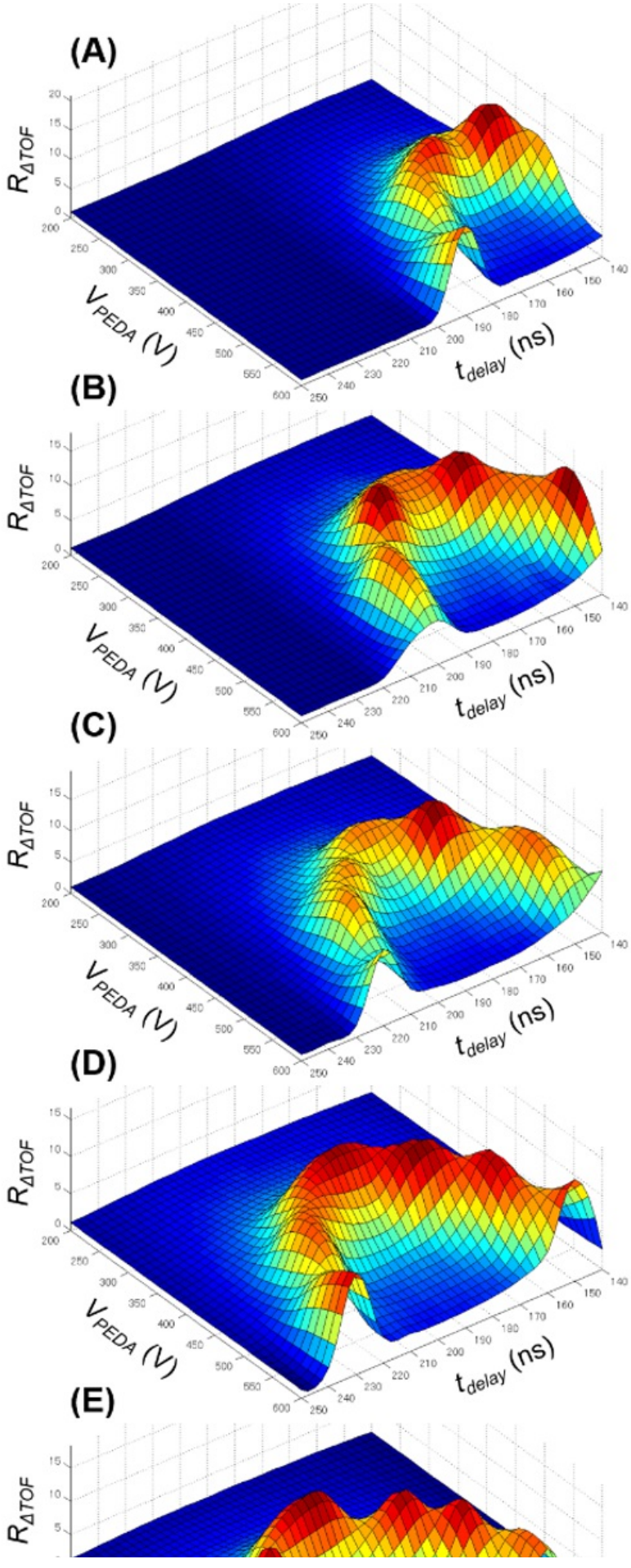
(A)
(B)
(C)
(D)
(E)
$R_{\Delta TOF}$
V_{PEDA} (V)
t_{delay} (ns)

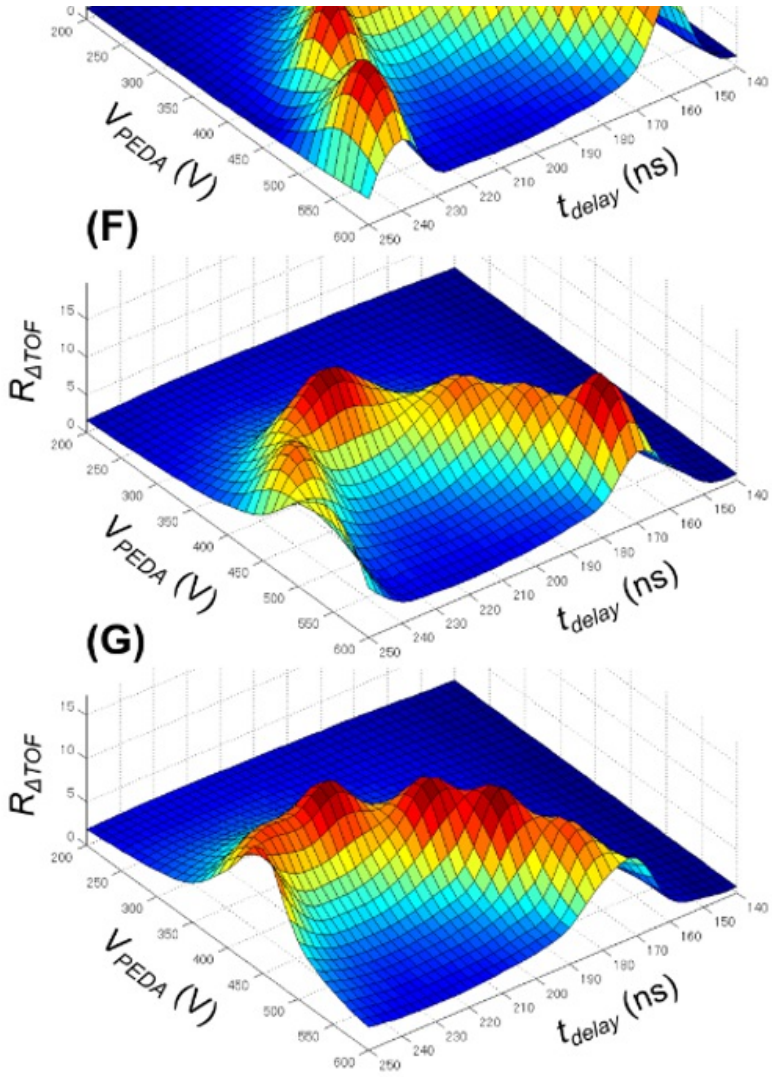

Figure 7. Reduction factor of time-of-flight dispersion as a function of V_{PEDA} and t_{delay}, examined by simulating trajectories of singly charged ions. (A) 70 Da, (B) 80 Da, (C) 90 Da, (D) 100 Da, (E) 110 Da, (F) 120 Da, (G) 130 Da.

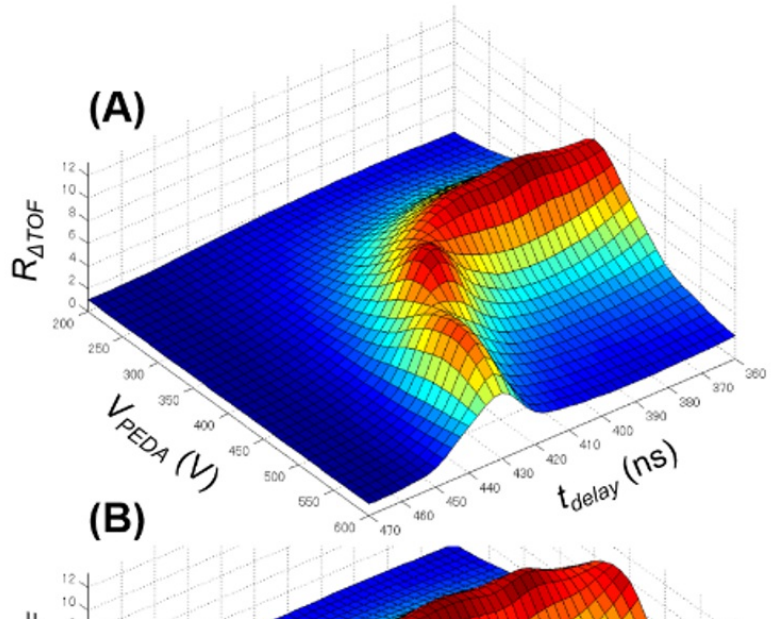

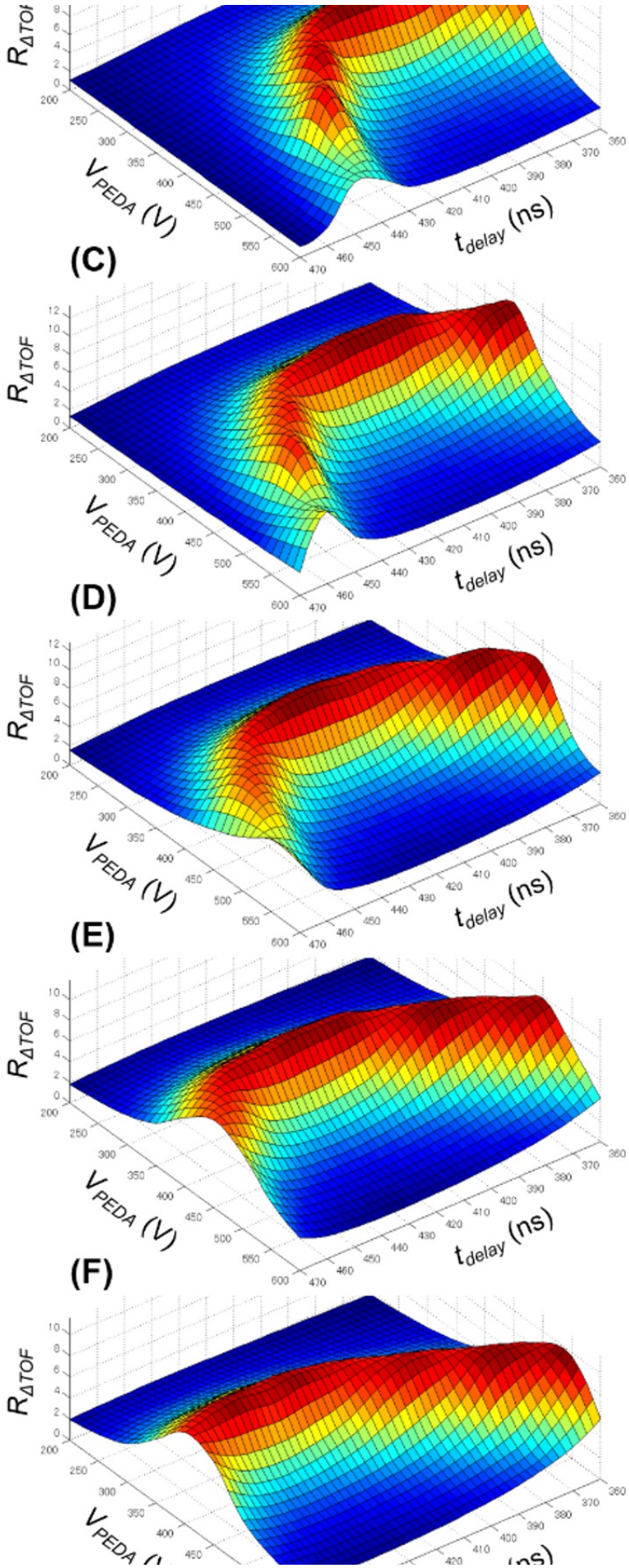
(C)
(D)
(E)
(F)
$R_{\Delta TOF}$
V_{PEDA} (V)
t_{delay} (ns)

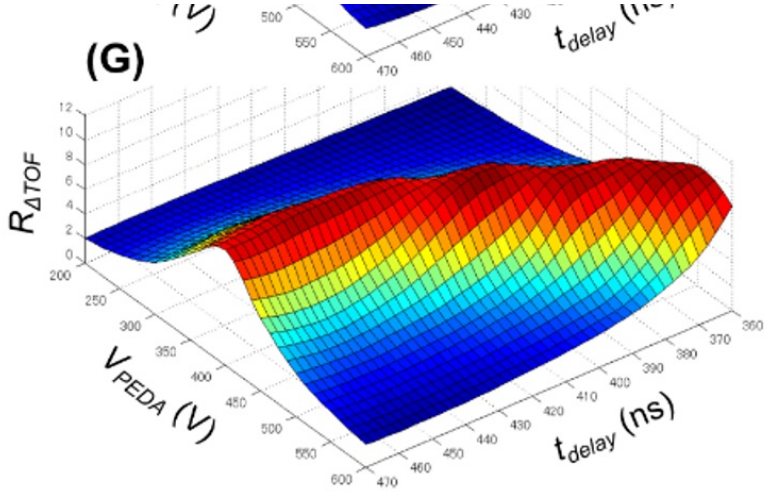

Figure 8. Reduction factor of time-of-flight dispersion as a function of V_{PEDA} and t_{delay}, examined by simulating trajectories of singly charged ions. (A) 340 Da, (B) 360 Da, (C) 380 Da, (D) 400 Da, (E) 420 Da, (F) 440 Da, (G) 460 Da.

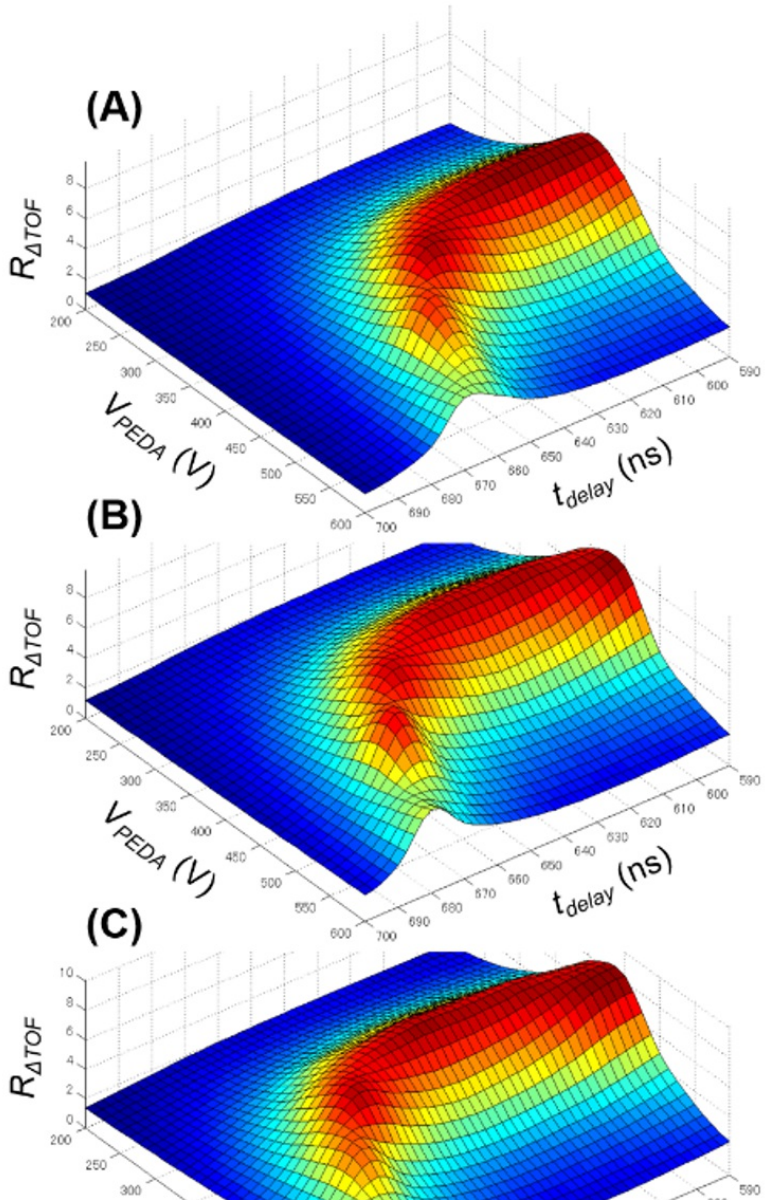

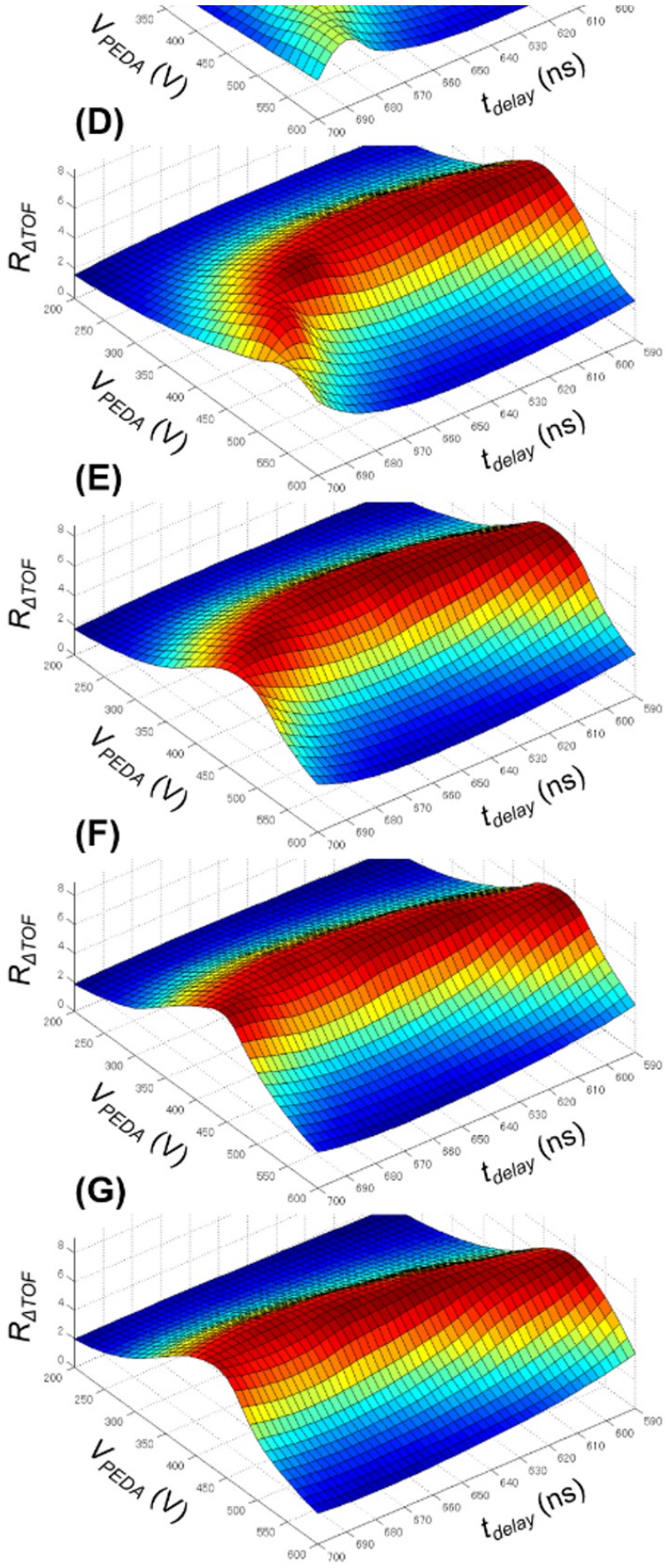

Figure 9. Reduction factor of time-of-flight dispersion as a function of V_{PEDA} and t_{delay}, examined by simulating trajectories of singly charged ions. (A) 810 Da, (B) 840 Da, (C)

870 Da, (D) 900 Da, (E) 930 Da, (F) 960 Da, (G) 990 Da.

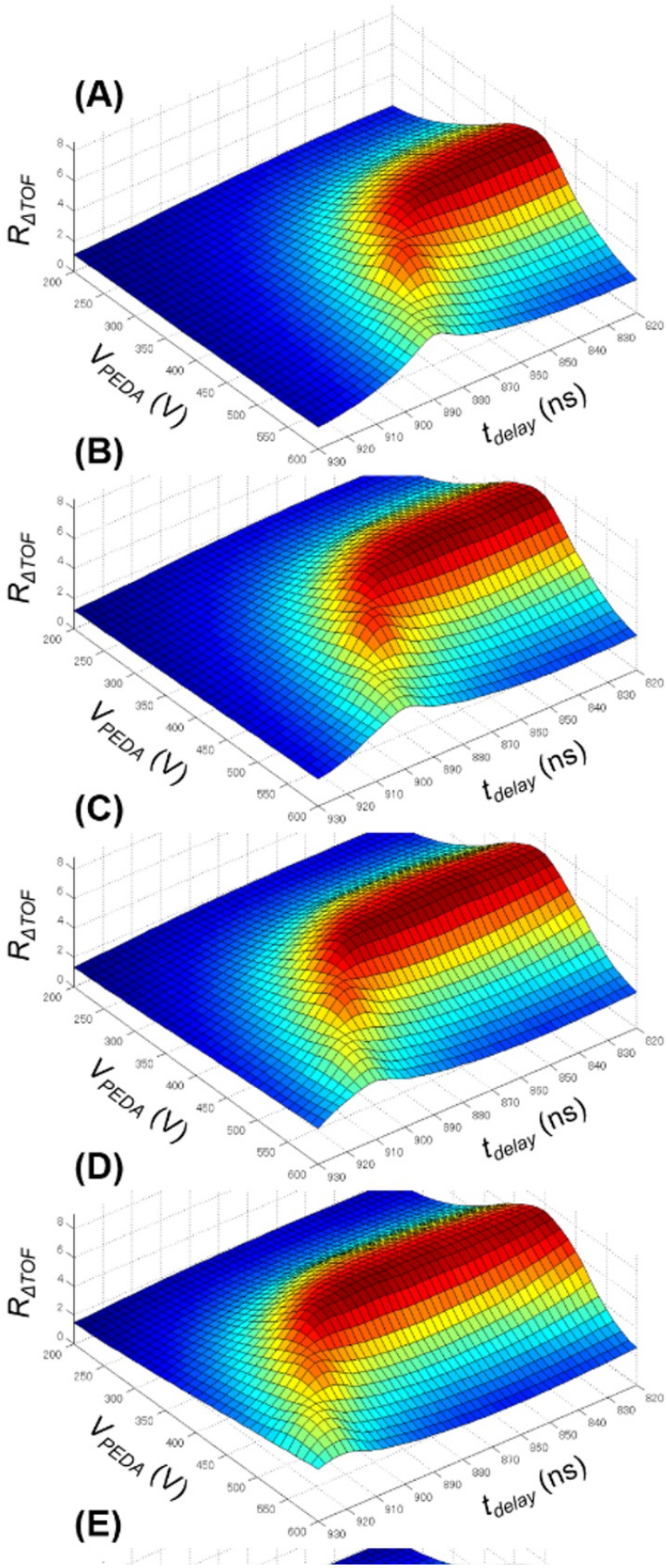

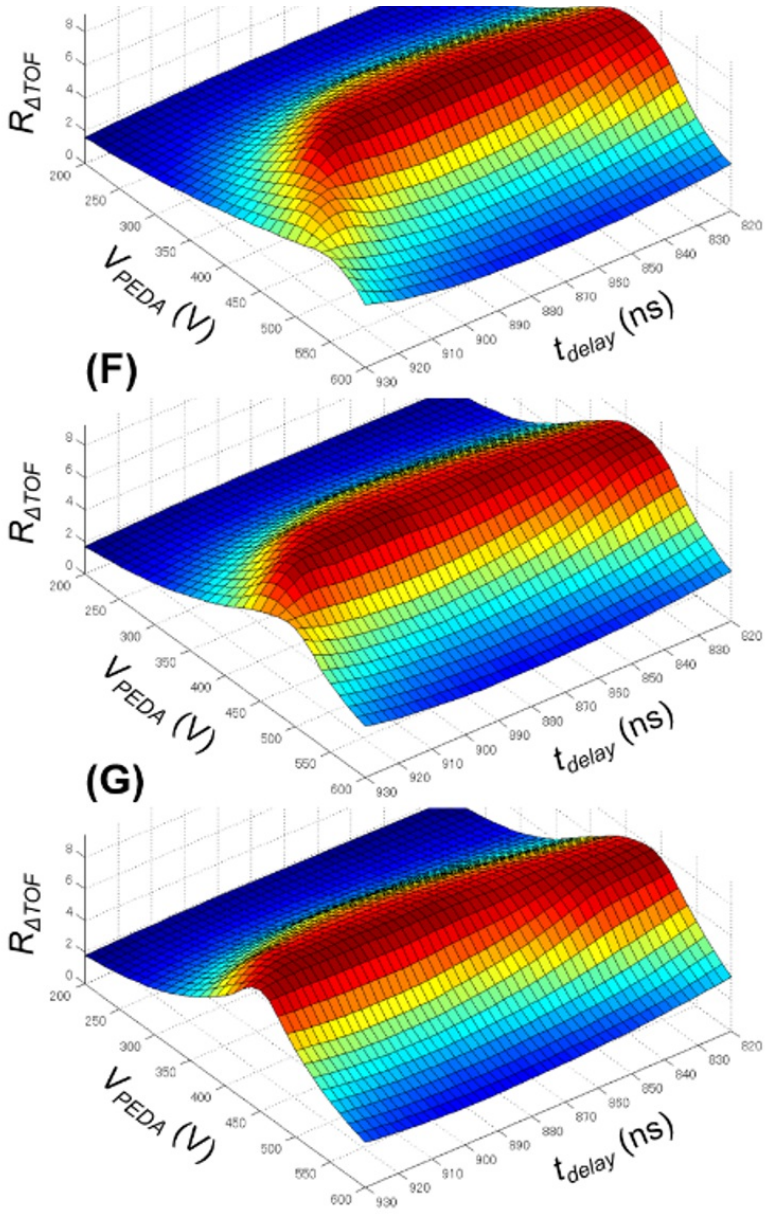

Figure 10. Reduction factor of time-of-flight dispersion as a function of V_{PEDA} and t_{delay}, examined by simulating trajectories of singly charged ions. (A) 1480 Da, (B) 1520 Da, (C) 1560 Da, (D) 1600 Da, (E) 1640 Da, (F) 1680 Da, (G) 1720 Da.

In the same way, the simulation results are shown in 3D plots for singly charged ions of 340–460 Da (Fig. 8), 810–990 Da (Fig. 9), and 1480–1720 Da (Fig. 10). The ranges of V_{PEDA} and t_{delay} for which the focusing effect can be obtained differ according to the mass regions.

3.3. Optimization of PEDA Parameters

From Figures 7–10, it can be seen that V_{PEDA} = 400 V is in the red region for every mass region. Considering this, the optimized PEDA parameters were explored by fixing V_{PEDA} at 400 V. Figure 11 is a graph plotting the square root of mass on the horizontal axis and t_{delay} at which the maximum $R_{\Delta TOF}$ was obtained on the vertical axis. There is a linear

relationship between the square root of mass and the optimal value of t_{delay}. Figure 12 shows the variation in $R_{\Delta TOF}$ for the narrow mass ranges in the vicinities of 100, 400, 900 and 1600 Da when the t_{delay} values optimized for these masses were applied to each mass region.

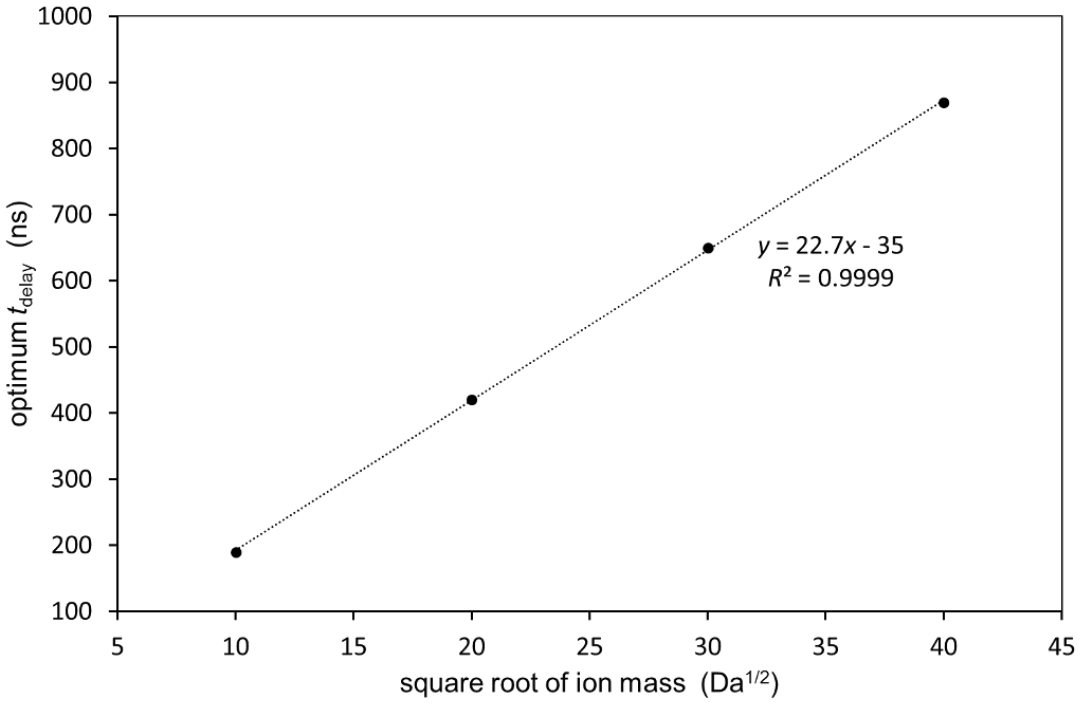

Figure 11. Linear correlation plots between square root of ion mass and the optimum t_{delay} that maximizes $R_{\Delta TOF}$ at the fixed value of V_{PEDA} = 400 V.

Because a certain setting of the optimized V_{PEDA} and t_{delay} combination is effective only for a narrow mass range (mass window), the PEDA parameters need to be adjusted according to the target mass window. In Figures 7–10, the optimal V_{PEDA} values given by the red regions close to minimum at V_{PEDA} = 400 V. Therefore, to adjust the PEDA parameters practically, an experimenter may find the optimal combination of t_{delay} and the minimum value of V_{PEDA} for a certain mass window first. Then for the other mass windows, the same value of V_{PEDA} is applied, and the optimal t_{delay} values are predicted by a linear relationship with the square root of mass values. This procedure is expected to avoid empirically determining the optimal PEDA parameters for every mass window.

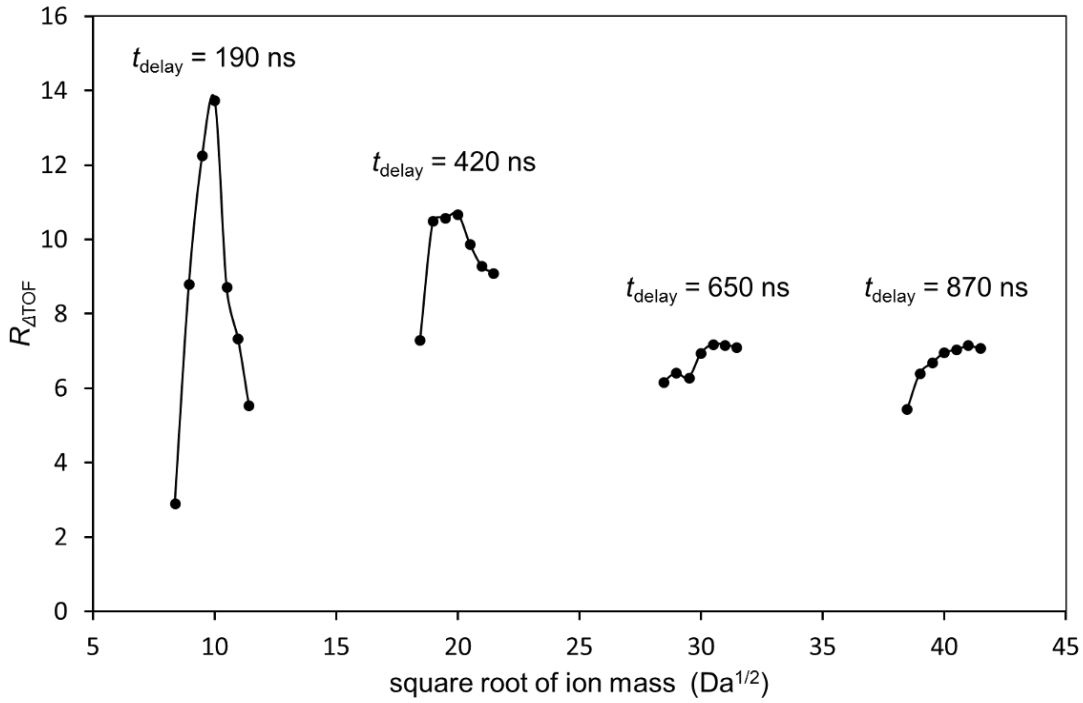

Figure 12. Variations in $R_{\Delta TOF}$ for narrow mass ranges at the fixed value of V_{PEDA} = 400 V. The annotated values of t_{delay} optimal for 100 Da, 400 Da, 900 Da and 1600 Da are applied to the corresponding mass ranges.

3.4. Effect of PEDA on Image Formation

As mentioned above, under conditions where the time-of-flight focusing effect of PEDA can be obtained, it is considered that PEDA may not affect the image formation because V_2 = 18.8 kV is maintained until the ions pass through the extract electrode. This assumption was verified by the simulation results. The ratio $R_{\Delta Z}$:

$R_{\Delta Z}$ = (ΔZ with PEDA) / (ΔZ without PEDA)

was used as an index for evaluating the image formation, where ΔZ is the spread of z-displacements on the detector. An $R_{\Delta Z}$ greater than 1 means a degradation of the imaging performance due to PEDA. Figure 13 is a graph plotting the square root of mass on the horizontal axis and $R_{\Delta Z}$ on the vertical axis. V_{PEDA} was fixed at 400 V, and the t_{delay} values as the same as in Figure 12 were applied. Except for the case of the initial location z_0 = 200 µm exhibits some degradation of the imaging performance at the high mass side, overall it can be said that the effect of PEDA on the image formation remains small.

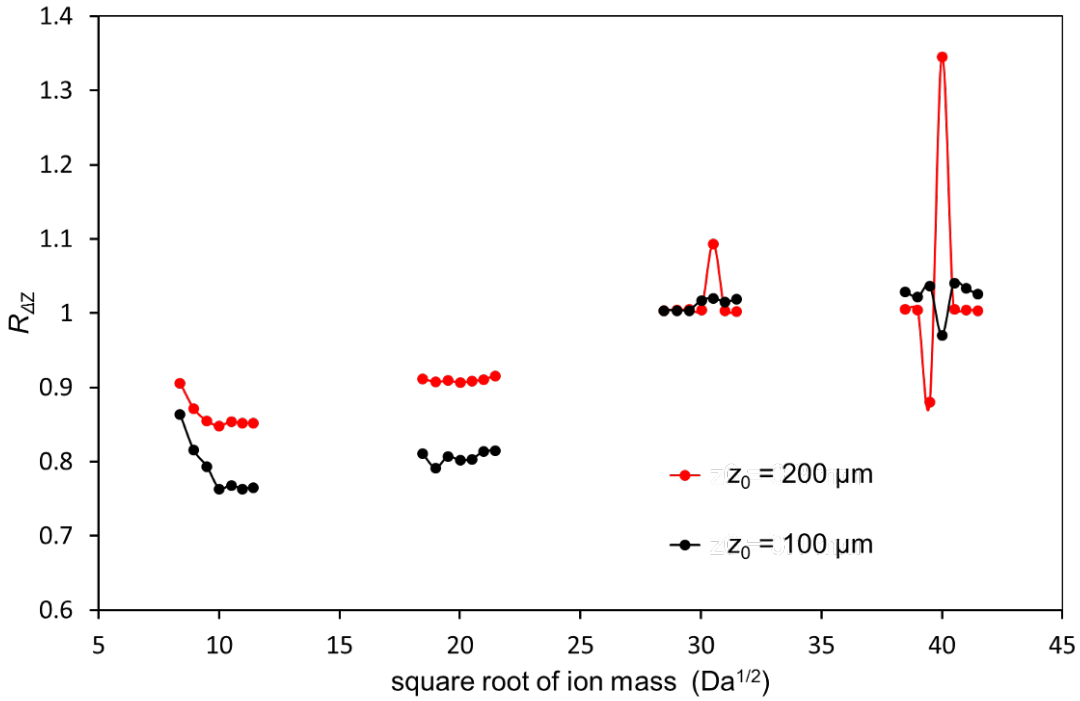

Figure 13. Variation in $R_{\Delta Z}$ obtained from two starting locations of ion trajectories at the same PEDA parameter settings as Fig. 12.

3.5. Effect of PEDA High-Voltage Rising Waveform

The rising waveform of voltage delivered from an actual electric circuit always has a time constant of a finite magnitude that is not zero. However, it is interesting what differences would arise on the results between the exponentially rising waveform and an ideal step function rising waveform in which the voltage switches instantaneously at time t_{delay}. An equally large set of simulations as above was conducted on the case where a step function was applied to the PEDA high-voltage rising waveform. When the step function rising waveform was used, the optimum values of the PEDA parameters were slightly different from those described above. Figure 14 is a graph appending the simulation results for the step function rising waveform with these optimal PEDA parameters to Figure 12. It is noteworthy that the mass window over which the time-of-flight focusing effect occurs is broader for the "realistic" exponentially rising waveform case than for the "ideal" step function one. Although further investigation of this phenomenon is necessary to make positive use for broadening the mass window, a similar effect has also been reported on the conventional delayed ion extraction in MALDI time-of-flight mass spectrometers[16]. Our future challenge is to explore, through simulations and experiments, the time constant of the exponentially rising waveform that can further expand the mass window.

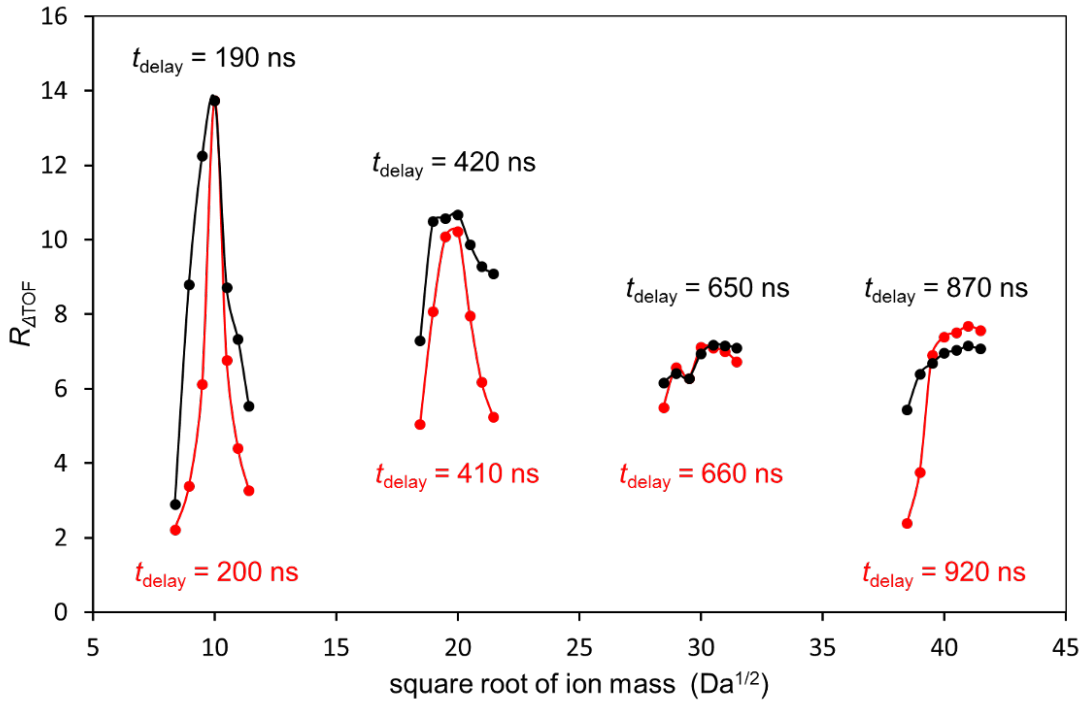

Figure 14. The results of PEDA with a step function rising waveform are appended as lines and markers in red to the same graph as Fig. 12. The optimal PEDA parameters for the case of the step function rising waveform are V_{PEDA} = 400 V and t_{delay} values annotated in red, slightly different from the case of the exponentially rising waveform.

3.6. Ion Trajectory Computational Quality

In SIMION, the methods to compute ion trajectories can be controlled by the numerical settings in the Trajectory Quality panel displayed on the Normal tab screen[17]. This parameter can be set to 0 or a positive or negative integer, of which sign alters the computation methods for ion trajectories. Basically, its larger absolute value higher the calculation accuracy at the cost of computation load. In this study, this parameter was set to 3 (the default value). To confirm the validity of setting value 3 for this parameter, the simulation results of larger setting values were validated for singly charged ions with masses from 340 Da to 460 Da. Figure 15 is a graph plotting the validation result, after all, almost no change was observed for the increased Trajectory Quality values. At the rightmost of the graph (the parameter set to 150), the computation time reached to about 30 times longer than the default setting. From this validation result, it can be concluded that the Trajectory Quality setting value 3 in the present study is appropriate, and that the detailed properties of PEDA found in the simulation results are not artifacts that can be caused by an insufficient computational quality.

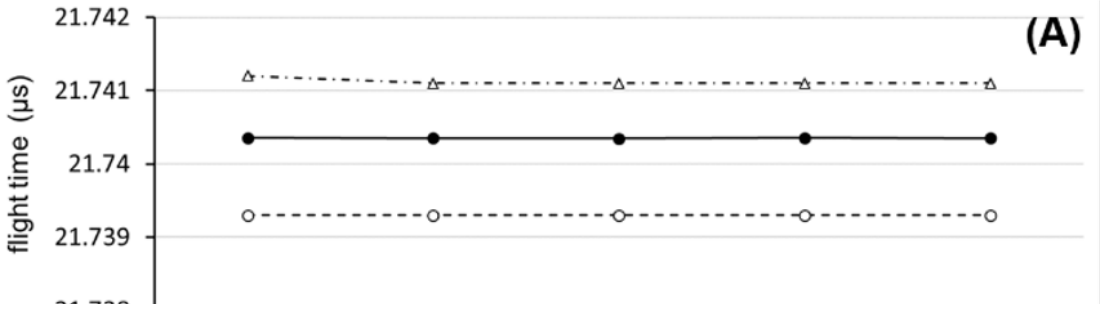

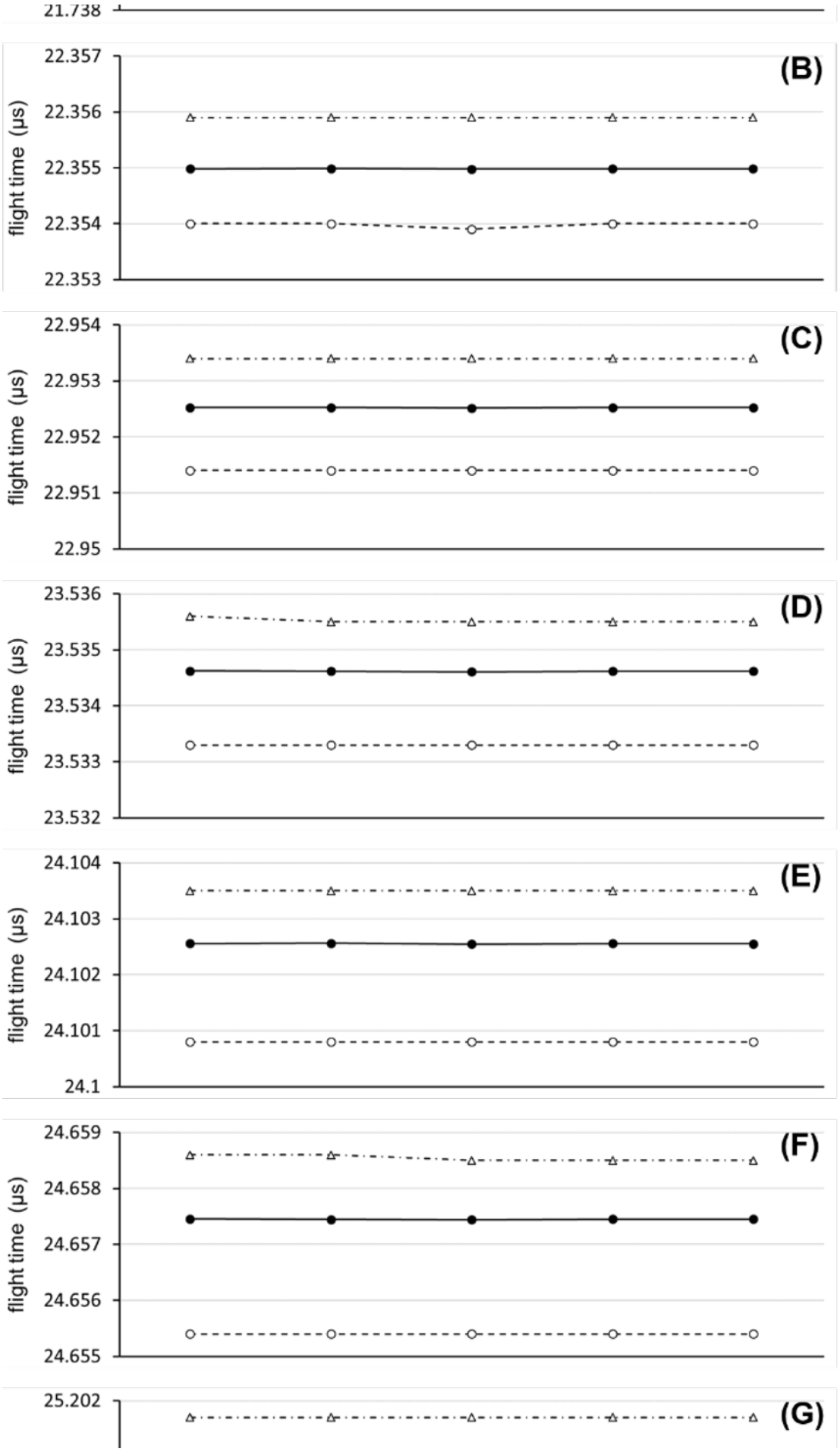
21.738
22.357
22.356
22.355
22.354
22.353
flight time (μs)
(B)
22.954
22.953
22.952
22.951
22.95
flight time (μs)
(C)
23.536
23.535
23.534
23.533
23.532
flight time (μs)
(D)
24.104
24.103
24.102
24.101
24.1
flight time (μs)
(E)
24.659
24.658
24.657
24.656
24.655
flight time (μs)
(F)
25.202
(G)

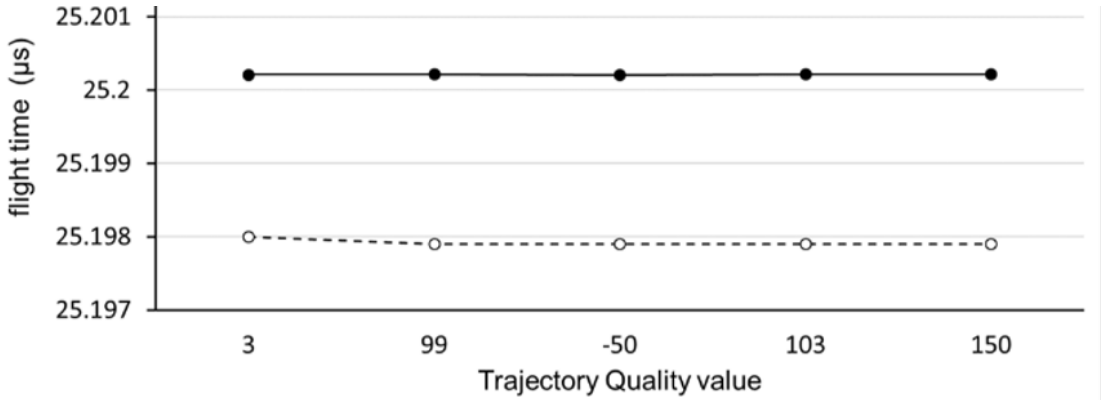

Figure 15. Flight times of singly charged ions whose masses are (A) 340 Da, (B) 360 Da, (C) 380 Da, (D) 400 Da, (E) 420 Da, (F) 440 Da and (G) 460 Da, respectively, calculated at various Trajectory Quality settings. V_{PEDA} = 400 V. t_{delay} = 420 ns. Filled circle, open circle and open triangle markers indicate average, minimum and maximum flight times, respectively.

The present simulation study supports good prospects for the realization of projection-type MSI based on the commercially available TOFMS equipment. The hardware modifications of Ultraflex for projection-type MSI experiments are being undertaken.

References

1. ^*Buchberger AR, DeLaney K, Johnson J, Li L. Mass spectrometry imaging: a review of emerging advancements and future insights. Anal Chem. 2018;90(1):240–265. doi:10.1021/acs.analchem.7b04733*
2. ^*Caprioli RM, Farmer TB, Gile J. Molecular imaging of biological samples: localization of peptides and proteins using MALDI-TOF MS. Anal Chem. 1997;69(23):4751–4760. doi:10.1021/ac970888i*
3. ^*Zavalin A, Yang J, Haase A, Holle A, Caprioli R. Implementation of a Gaussian beam laser and aspheric optics for high spatial resolution MALDI imaging MS. J Am Soc Mass Spectrom. 2014;25(6):1079–1082. doi:10.1007/s13361-014-0872-5*
4. ^*Luxembourg SL, Mize TH, McDonnell LA, Heeren RMA. High-spatial resolution mass spectrometric imaging of peptide and protein distributions on a surface. Anal Chem. 2004;76(18):5339–5344. doi:10.1021/ac049692q*
5. ^*Hazama H, Aoki J, Nagao H, Suzuki R, Tashima T, Fujii K, Masuda K, Awazu K, Toyoda M, Naito Y. Construction of a novel stigmatic MALDI imaging mass spectrometer. Appl Surf Sci. 2008;255(4):1257–1263. doi:10.1016/j.apsusc.2008.05.058*
6. ^*Burleigh RJ, Guo A, Smith N, Green A, Thompson S, Burt M, Brouard M. Microscope imaging mass spectrometry with a reflectron. Rev Sci Instrum. 2020;91(2):023306. doi:10.1063/1.5142271*
7. ^*Oelsner A, Schmidt O, Schicketanz M, Klais M, Schönhense G, Mergel V, Jagutzki O, Schmidt-Böcking H. Microspectroscopy and imaging using a delay line detector in time-of-flight photoemission microscopy. Rev Sci Instrum. 2001;72(10):3968–3974. doi:10.1063/1.1405781*

8. ^*Hayashi M, Naito Y. Development of an efficient ion detection technique for microscope mode imaging mass spectrometry using a delay line detector. J Mass Spectrom Soc Jpn. 2011;59(2):23–33. (in Japanese) doi:10.5702/massspec.59.23*
9. ^*Winter B, King SJ, Brouard M, Vallance C. A fast microchannel plate-scintillator detector for velocity map imaging and imaging mass spectrometry. Rev Sci Instrum. 2014;85(2):023306. doi:10.1063/1.4866647*
10. ^*Nomerotski A. Imaging and time stamping of photons with nanosecond resolution in Timepix based optical cameras. Nucl Instrum Methods Phys Res Sect A. 2019;937(1):26–30. doi:10.1016/j.nima.2019.05.034*
11. ^*Hirao T, Naito Y. Development and verification of Ion Camera realizing ultrafast microscope-mode mass spectrometry imaging. J Mass Spectrom Soc Jpn. 2021;69(3):46–57. (in Japanese) doi:10.5702/massspec.21-118*
12. ^*Schueler BW. Microscope imaging by time-of-flight secondary ion mass spectrometry. Microsc Microanal Microstruct. 1992;3(2-3):119–139. doi:10.1051/mmm:0199200302-3011900*
13. ^*Aoki J, Hazama H, Toyoda M. Novel ion extraction method for imaging mass spectrometry. J Mass Spectrom Soc Jpn. 2011;59(3):57–61. doi:10.5702/massspec.11-20*
14. ^*Guo A, Burt M, Brouard M. Mass-resolved ion microscope imaging over expanded mass ranges using double-field post-extraction differential acceleration. Int J Mass Spectrom. 2018;429:121–126. doi:10.1016/j.ijms.2017.06.010*
15. ^*Dreisewerd K. The desorption process in MALDI. Chem Rev. 2003;103(2):395–426. doi:10.1021/cr010375i*
16. ^*Franzen J. Improved resolution for MALDI-TOF mass spectrometers: a mathematical study. Int J Mass Spectrom. 1997;164(1-2):19–34. doi:10.1016/S0168-1176(97)00049-9*
17. ^*Dahl DA. SIMION 3D version 7.0 user's manual. Appendix E. Bechtel Bwxt Idaho, LLC, Idaho Falls, ID, 2000.*